Ehlers *et al. Breast Cancer Research* (2025) 27:14
https://doi.org/10.1186/s13058-025-01964-4

Breast Cancer Research

RESEARCH Open Access

Natural killer cells occupy unique spatial neighborhoods in HER2$^-$ and HER2$^+$ human breast cancers

Femke A. I. Ehlers[1,2,3], Katie E. Blise[4], Courtney B. Betts[5], Shamilene Sivagnanam[5], Loes F. S. Kooreman[3,6], E. Shelley Hwang[7], Gerard M. J. Bos[2,3], Lotte Wieten[1,3*] and Lisa M. Coussens[5,8,9*]

Abstract

Tumor-infiltrating lymphocytes are considered clinically beneficial in breast cancer, but the significance of natural killer (NK) cells is less well characterized. As increasing evidence has demonstrated that the spatial organization of immune cells in tumor microenvironments is a significant parameter for impacting disease progression as well as therapeutic responses, an improved understanding of tumor-infiltrating NK cells and their location within tumor contextures is needed to improve the design of effective NK cell-based therapies. In this study, we developed a multiplex immunohistochemistry (mIHC) antibody panel designed to quantitatively interrogate leukocyte lineages, focusing on NK cells and their phenotypes, in two independent breast cancer patient cohorts ($n=26$ and $n=30$). Owing to the clinical evidence supporting a significant role for NK cells in HER2$^+$ breast cancer in mediating responses to Trastuzumab, we further evaluated HER2$^-$ and HER2$^+$ specimens separately. Consistent with literature, we found that CD3$^+$ T cells were the dominant leukocyte subset across breast cancer specimens. In comparison, NK cells, identified by CD56 or NKp46 expression, were scarce in all specimens with low granzyme B expression indicating reduced cytotoxic functionality. Whereas NK cell density and phenotype did not appear to be influenced by HER2 status, spatial analysis revealed distinct NK cells phenotypes regarding their proximity to neoplastic tumor cells that associated with HER2 status. Spatial cellular neighborhood analysis revealed multiple unique neighborhood compositions surrounding NK cells, where NK cells from HER2$^-$ tumors were more frequently found proximal to neoplastic tumor cells, whereas NK cells from HER2$^+$ tumors were instead more frequently found proximal to CD3$^+$ T cells. This study establishes the utility of quantitative mIHC to evaluate NK cells at the single-cell spatial proteomics level and illustrates how spatial characteristics of NK cell neighborhoods vary within the context of HER2$^-$ and HER2$^+$ breast cancers.

Keywords NK cells, Breast cancer, Immune contexture, Multiplex immunohistochemistry

Lotte Wieten and Lisa M. Coussens Co-senior authors and corresponding authors.

*Correspondence:
Lotte Wieten
l.wieten@mumc.nl
Lisa M. Coussens
coussenl@ohsu.edu

Full list of author information is available at the end of the article

Introduction

Breast cancer is the most common cancer in women, and although survival rates have improved, it remains a leading cause of death [1]. Based on their molecular classification, breast cancer subtypes are largely segregated into basal-like, luminal A, luminal B, normal-like, and HER2$^+$ breast cancer subtypes and guide therapeutic decisions [2]; however, even within subtypes, high heterogeneity is recognized. Tumor-infiltrating lymphocytes are generally accepted to be important for favorable therapeutic responses, but the significance of natural killer (NK) cells in breast cancer is less well characterized [3]. NK cells are cytotoxic leukocytes that can impact neoplastic cells through an extensive array of cell surface receptors, with one of the most potent activating receptors being CD16A (FcγRIIIA), which binds immunoglobulins and immune complexes, as well as tumor-targeting antibodies that induce tumor cell killing through antibody-dependent cellular cytotoxicity (ADCC) [4, 5]. In addition to their cytotoxic capabilities, NK cells release proinflammatory cytokines and chemokines to activate and recruit other immune cell types, including dendritic cells and macrophages [6, 7].

NK cell abundance and functional status are positively correlated with improved clinical outcomes in several solid tumor types, supporting the tenet that NK cells are critical for tumor control despite their relatively low frequency (reviewed in [8, 9]). In experimental mouse models of HER2$^+$ breast cancer, NK cells were reported to significantly contribute to the efficacy of the anti-HER2 antibody Trastuzumab by mediating ADCC [10, 11]. Indirect evidence further supports that NK cells also contribute to the efficacy of Trastuzumab in patients with HER2$^+$ breast cancer, as demonstrated by increased tumor-infiltrating NK cells following Trastuzumab therapy [12–14].

Due to their cytotoxic potential and high safety profile, NK cells are promising candidates for adoptive cell therapy [15]. However, tumor-infiltrating NK cells are frequently described as dysfunctional, which might underlie the limited success of adoptive NK cell therapy in breast cancer [16]. NK cell effector functions can be inhibited by neoplastic tumor cells through the downregulation of activating ligands and the expression of inhibitory ligands such as HLA class I [17]. Moreover, the immunosuppressive tumor microenvironment (TME) is known to negatively affect NK cells via various mechanisms, including immunosuppressive cytokines and hypoxic conditions [18]. Hypoxia is frequently present in solid tumors and has been reported in 50% of breast cancer patients [19]. Compared with blood, tumor-infiltrating NK cells express low levels of activating receptors and have low cytotoxic potential, indicating that these alterations could be TME-mediated [20, 21].

Strategies to enhance NK cell anti-tumor responses include cytokine activation and NK cell-engaging molecules directed against inhibitory checkpoint molecules to prevent NK cell inactivation or designed to stimulate NK cell activation and ADCC [15]. The combination of anti-HER2 targeting therapy e.g., Trastuzumab, with NK cell-based therapy could be an approach to increase NK cell activity in HER2$^+$ breast cancer [22]. In addition to enhancing NK cell potency, it is therefore crucial to understand immune cell spatial parameters the TMEs, including distribution of endogenous NK cells and their interactions with neoplastic tumor cells, as well as other tumor-infiltrating leukocytes. Cellular and spatial heterogeneity has been linked to clinical outcomes in breast cancer; spatial organization of immune cells within the TME of triple-negative breast cancers (assessed by multiplexed ion beam imaging by time-of-flight, MIBI-TOF), was linked to overall patient survival [23, 24]. Moreover, using multiplex immunohistochemistry [25, 26], we reported functional immune contextual changes in paired-biopsies following adjuvant therapy in polyclonal breast cancer metastases revealing the impact of therapy linked to organ-specific leukocyte heterogeneity and distribution [27]. However, little is known regarding infiltration and distribution of NK cells within heterogeneous breast cancer TMEs. Common to the above-described studies evaluating NK cells in human breast cancer, flow cytometry and standard single-color immunohistochemistry (IHC) have been utilized for leukocyte quantitation, but have not reported contexture of NK cell neighborhoods or their NK cell functional state. Herein, to fill in these gaps, we utilized multiplex IHC (mIHC) methodology to reveal in situ phenotyping and spatial architectures of diverse NK cell neighborhoods [28] utilizing a novel panel of antibodies to quantify leukocyte lineages, including deep-auditing NK cells and their phenotypes, as well as their spatial architecture in human HER2$^-$ and HER2$^+$ breast cancers to improve strategies for NK cell-based therapy.

Materials and methods

Clinical samples

Cohort 1: Breast cancer tissue was obtained from Duke University, Durham, USA, and shipped to Oregon Health & Science University (OHSU), Portland OR, USA. The study protocol was approved by the IRB of Duke University (Durham, NC USA) ethics committee as appropriate (Pro00034242). Informed consent was obtained from all human subjects included in this study. *Cohort 2*: Breast cancer tissue was obtained by Maastricht University Medical Center+, Maastricht, The Netherlands. The collection, storage, and use of tissue and patient data were performed in agreement with the "Code for Proper Secondary Use of Human Tissue in the Netherlands"

and approved by the local ethics committee (METC 2019 – 1154). The clinical characteristics of both cohorts are shown in Supplementary Table S2.

Multiplex immunohistochemistry and image acquisition

Multiplex immunohistochemistry (mIHC) was performed as previously described [25, 26]. Briefly, formalin-fixed, paraffin-embedded (FFPE) tissue sections (5 µm) were baked in a 60 °C heat chamber for 30 min, deparaffinized in xylene and rehydrated in serially graded ethanol and placed in water. After deparaffinization, the slides were fixed in 10% neutral buffered formalin for 30 min and subsequently washed twice in PBS to prevent tissue from falling of the slides [29]. Tissue slides were counterstained with hematoxylin (Dako, S3301) for 1 min at room temperature (RT), washed in water, and mounted with 1X TBST buffer (Boston Bioproducts, IBB-181R) before coverslips (Thermo Scientific, 12460 S) were placed on the slides. Slides were scanned using the whole slide digital scanner Aperio ImageScope AT (Leica Biosystems) at 20X magnification. Coverslips were removed by placing slides in TBST for a few minutes with agitation. For heat-mediated antigen retrieval, slides were placed in 1X EDTA Decloaker (Biocare Medical, CB917) in a pressure cooker for 15–20 min at 115 °C for staining cycles 1 and 3, and slides were placed in 1X citrate buffer, pH 6.0 (Biogenex Laboratories, HK080) for 20 min at 95 °C for the other staining cycles (Supplementary Table S1). After antigen retrieval and washing in water and TBST, slides were incubated with dual endogenous peroxidase block (Dako, S2003) for 10 min at RT. Protein blocking was performed with 5% normal goat serum and 2.5% BSA in PBS for 10 min at RT. Slides were incubated with the primary antibody for 30–60 min at RT or overnight at 4 °C. After slides were washed, they were incubated with the secondary antibody Histofine Simple Stain MAX PO horseradish peroxidase-conjugated polymer (Nichirei Biosciences, 414134–414144 F) for 30 min at RT in all staining rounds, except cycle 3 round 2 where slides were incubated for 60 min at RT with histofine. Information on antibodies and staining conditions is listed in Supplementary Table S1. Chromogenic signal detection was performed with AEC substrate kit, Peroxidase (Vector Laboratories, SK-4200) for all antibodies, except the anti-PD-1 antibody that was detected with AMEC Red Substrate, Peroxidase (Vector Laboratories, SK-4285). Slides were scanned using the whole slide digital scanner and coverslips were removed, as described above. AEC or AMEC were removed by placing the slides in serially graded ethanol. For cycles with two rounds of antibody development, horseradish peroxidase was inactivated by incubation with dual endogenous peroxidase block (Dako, S2003) for 10 min at RT. Protein blocking was repeated before each following antibody was added. For the following cycles, the same steps from antigen retrieval to slide scanning were performed as described above. Heat-mediated antigen retrieval stripped the antibodies from the previous staining cycle. Human tonsil and spleen were used as controls in all staining cycles and a representative visualization of each antibody is shown in Supplementary Figure S1.

ROI selection and image processing

In cohort 1, tissue area was limited and all intact regions were captured in 1–6 regions of interest (ROIs). In cohort 2, 4–13 ROIs with lymphoid aggregates, tumor-sparse areas and tumor-dense areas were selected. When tissue size allowed, several ROIs with a minimum of 0.8 mm^2 were selected to reflect tissue heterogeneity. For each specimen, the sum of the ROIs was used for subsequent calculations. Image co-registration and processing were performed as previously described [25, 30]. Cell percentages of immune cell lineages, presented in Fig. 1, were quantified via image cytometry gating strategies (Supplementary Figure S2).

Cellular neighborhood clustering analysis

A cellular neighborhood clustering analysis was performed, following steps similar to those previously described [31]. Briefly, we identified all cells, excluding "other nucleated cells", within a given distance threshold for every given seed cell phenotype across the dataset. In this study, we set the distance threshold to 60 µm and set the seed cell phenotype to be all NK cells. After computing the neighboring cells for each NK cell in the dataset, we then performed K-means clustering on the neighborhoods, using the normalized composition of cells comprising the neighborhoods as the features on which to cluster. The elbow method was used to determine the optimal number of clusters to generate clusters of neighborhoods, all of which possess similar cellular compositions surrounding NK cells.

Statistical analysis

Mann-Whitney-U tests were used to determine statistically significant differences for comparisons between two groups, and Benjamini-Hochberg correction was used to account for multiple hypothesis testing. Kruskal-Wallis tests were used to determine statistically significant differences for comparisons between multiple groups and *p*-values were adjusted for multiple comparisons via Dunn's adjustment. p-values < 0.05 were considered statistically significant and are reported as * $p < 0.05$ and ** $p < 0.01$. Spearman correlation coefficient was used to determine correlations of cell densities. Statistical analysis was performed using GraphPad software (version 9.2.0).

A

Cell types	Identification
Epithelial cells	$CD45^-$ $PanCK^+$
$CD8^+$ T cells	$CD45^+$ $CD3^+$ $CD8^+$
$CD4^+$ T cells	$CD45^+$ $CD3^+$ $CD8^-$
NK cells	$CD45^+$ $CD3^-$ $CD56^+$ $NKp46^+$ $CD45^+$ $CD3^-$ $CD56^+$ $NKp46^-$ $CD45^+$ $CD3^-$ $CD56^-$ $NKp46^+$
Myelomonocytic cells	$CD45^+$ $CD3^-$ $CD56^-$ $NKp46^-$ $CD11b^+$ $CD68^+$ $CD45^+$ $CD3^-$ $CD56^-$ $NKp46^-$ $CD11b^-$ $CD68^+$
Dendritic cells	$CD45^+$ $CD3^-$ $CD56^-$ $NKp46^-$ $CD11b^+$ $CD68^-$ $CD11c^+$ $CD45^+$ $CD3^-$ $CD56^-$ $NKp46^-$ $CD11b^-$ $CD68^-$ $CD11c^+$
Other myeloid cells	$CD45^+$ $CD3^-$ $CD56^-$ $NKp46^-$ $CD11b^+$ $CD68^-$ $CD11c^-$
Other $CD45^+$ cells	$CD45^+$ $CD3^-$ $CD56^-$ $NKp46^-$ $CD11b^-$ $CD68^-$ $CD11c^-$

Cell function	Identification
Proliferation	Ki67
Cytotoxicity	Granzyme B (GRZB)
NK cell activation and maturation	CD16, CD57, NKG2D
Immunoregulatory	PD-1, PD-L1, TIM-3, HLA class I
Hypoxia	Carbonic anhydrase IX (CAIX)

B

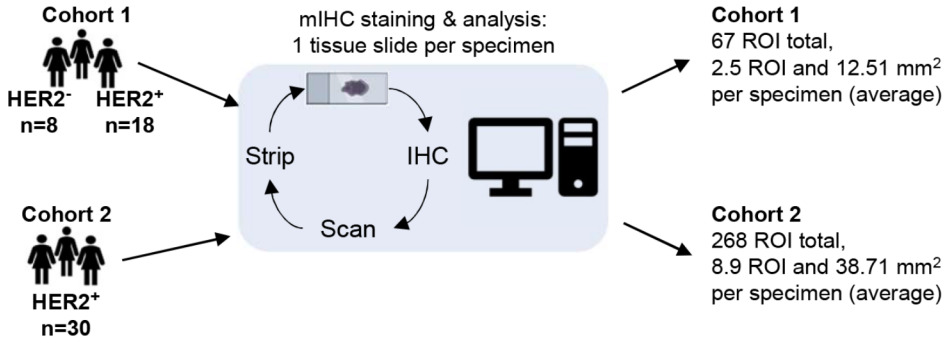

C

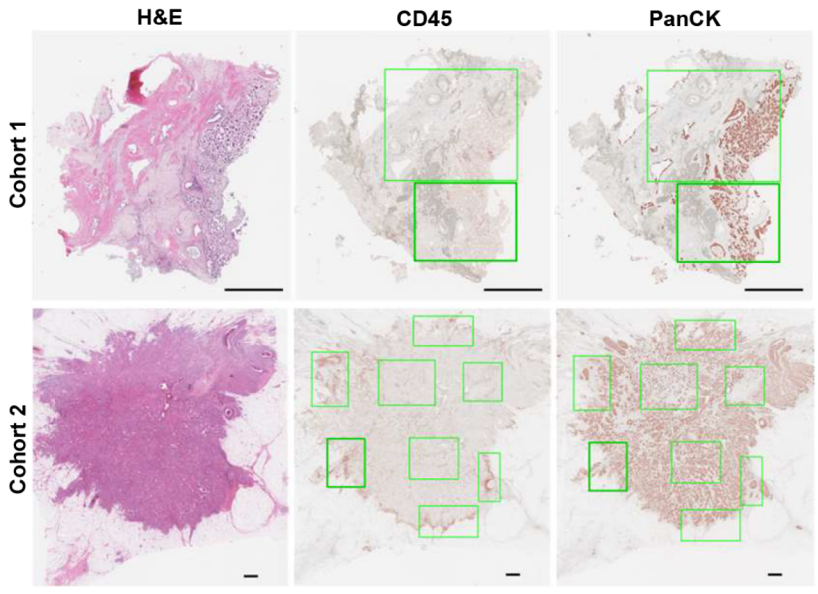

Fig. 1 Overview of identified cell types and human breast cancer specimens. **(A)** Cell types and corresponding markers that were used to identify the cell types. **(B)** Breast cancer cohorts evaluated in this study. HER2 status was assessed by IHC (cohort 1) or FISH (cohort 2). **(C)** Example images of H&E sections, CD45, and PanCK staining with the selected ROIs represented by the green boxes. Depending on tissue size, 1–6 ROI per specimen were analyzed in cohort 1, and 1–11 ROI per specimen were analyzed in cohort 2. In all images, scale bar = 1.0 mm. H&E = hematoxylin and eosin, ROI = region of interest

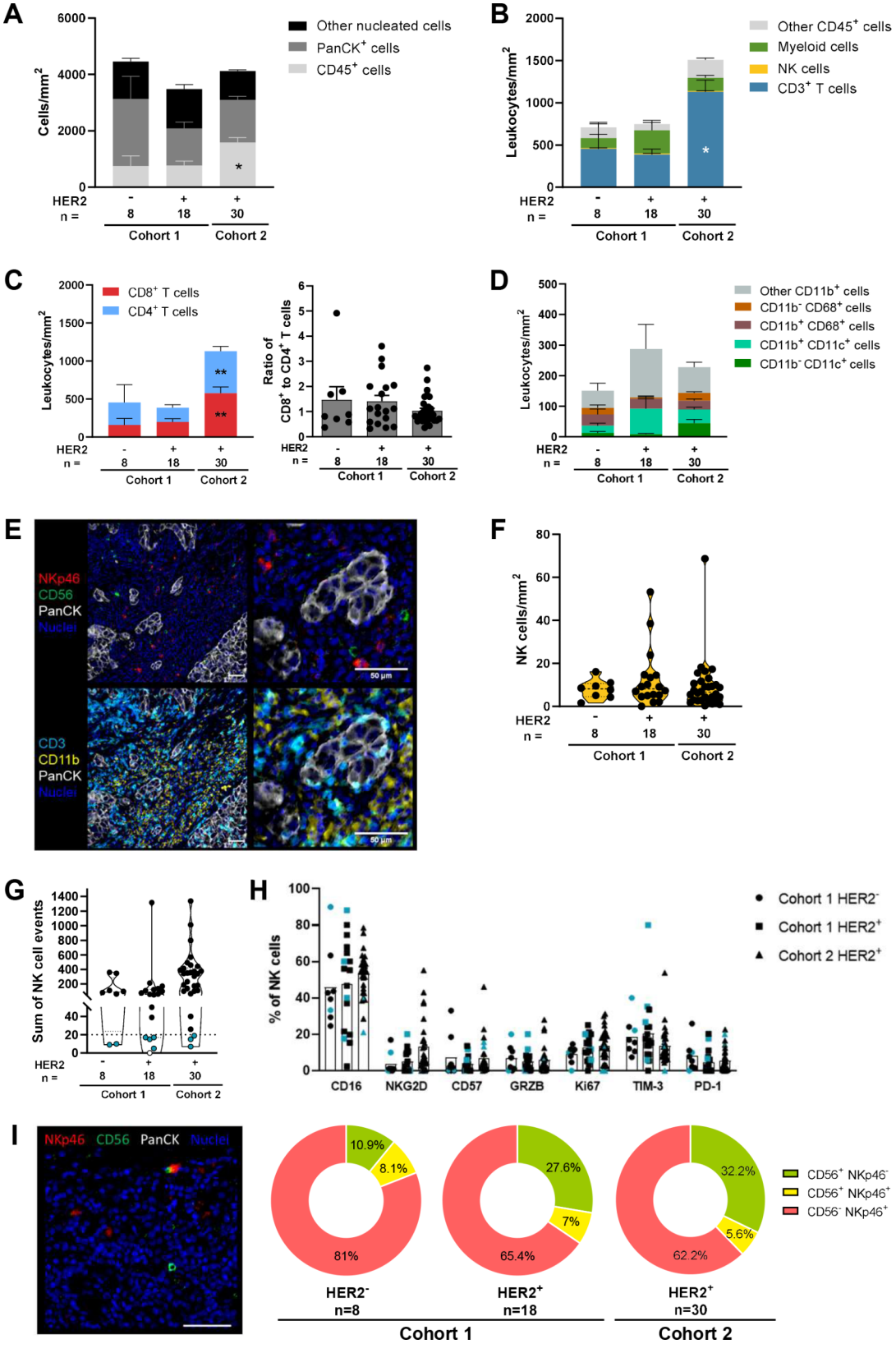

Fig. 2 (See legend on next page.)

(See figure on previous page.)

Fig. 2 Immune cell contexture in HER2$^-$ vs. HER2$^+$ breast cancer specimens. **(A)** Cell densities (cells/mm^2) of CD45$^+$ leukocytes, PanCK$^+$ epithelial cells, and other nucleated cells in cohort 1 (HER2$^-$ & HER2$^+$) and in cohort 2 (HER2$^+$). **(B)** Leukocyte densities of CD3$^+$ T cells, NK cells (CD3$^-$ CD56$^+$ NKp46$^-$ cells, CD3$^-$ CD56$^+$ NKp46$^+$ cells, and CD3$^-$ CD56$^-$ NKp46$^+$ cells), myeloid cells (comprising the five cell types detailed in **D**) and other CD45$^+$ leukocytes. **(C)** CD8$^+$ and CD4$^+$ T cell densities (left) and their ratio (right). **(D)** Dendritic cells (CD11b$^+$ CD11c$^+$ cells, CD11b$^-$ CD11c$^+$ cells), myelomonocytic cells (CD11b$^+$ CD68$^+$ cells, CD11b$^-$ CD68$^+$ cells), and other CD11b$^+$ myeloid cells. Kruskal-Wallis test with Dunn correction was used to determine differences in cell population densities in the three specimen groups. Bars indicate the mean ± SEM per cell population. Statistical significance between cohort 2 and both groups of cohort 1. **(E)** Pseudocolored image of one HER2$^+$ specimen (cohort 2) with a comparatively high density of NK cells, identified by either NKp46 or CD56 (upper panels). Density of CD3$^+$ T cells and CD11b$^+$ myeloid cells of the same region in lower panels, together with PanCK$^+$ epithelial cells and nuclear stain (Hematoxylin) in both images. Scale bars are 50 µm. **(F)** NK cell densities with one dot representing one tumor specimen. Per specimen, the sum of 1–11 ROIs per mm^2 was calculated. **G-H)** One dot represents one tumor specimen. Those with < 20 events are indicated by cyan color. In one specimen (open circle), no NK cells were detected. Sum of NK cell events from all analyzed ROIs (**G**). Expression of NK cell markers as % of total NK cells (**H**). **I)** Image with a CD56$^+$ NKp46$^-$ NK cell, CD56$^-$ NKp46$^+$ NK cells, and CD56$^+$ NKp46$^+$ double-positive NK cells, scale bar = 50 µm (left). The three identified NK cell subpopulations are depicted as % of total NK cells (right)

Results

Immune cell context in human breast cancer specimens

To identify NK cells and their phenotypes in human breast cancer, we used a previously validated mIHC platform and antibody panels designed to elaborate leukocyte lineages, including the presence and effector status of NK cells. A single FFPE tumor section per patient was sequentially stained with the mIHC panel, consisting of 20 well-validated antibodies (Suppl. Table S1). Chromogenic detection of antibodies in their respective cycles in the mIHC panel is shown in Suppl. Figure S1. Scanned images were quantitatively analyzed by image cytometry and identified cell types, alongside their functional biomarkers, are depicted (Fig. 1A, Suppl. Figure S2) [25, 26].

Based on the evidence for NK cells in HER2$^+$ breast cancer [10–14], we profiled NK cells in HER2$^-$ and HER2$^+$ tumor specimens from two independent patient cohorts, presented as cohort 1 consisting of both HER2$^-$ and HER2$^+$ specimens classified by standard IHC, and cohort 2 comprising solely HER2$^+$ therapy-naive breast cancer specimens, classified as HER2-amplified by FISH during diagnostic procedures (Fig. 1B). Patient characteristics of both cohorts are provided in Suppl. Table S2. We analyzed regions of interest (ROI) in tumor tissue areas that remained after all staining cycles were completed, and due to tissue availability, more ROIs were analyzed in cohort 2 (Fig. 1C, Suppl. Table S3). On average 12.5 mm^2 per tumor specimens were available for analysis in cohort 1, whereas 38.7 mm^2 per tumor specimens were available for analysis in cohort 2, including areas with high leukocyte density potentially reflecting lymphoid aggregates (Fig. 1B-C).

We first evaluated CD45$^+$ leukocytes, pan-cytokeratin (PanCK)$^+$ epithelial cells and other nucleated cell densities. In cohort 1, the most abundant cells in HER2$^-$ specimens reflected PanCK$^+$ epithelial cells, as compared to the median of HER2$^+$ specimens, where PanCK$^+$ epithelial cells represented comparable density to other nucleated cells (Fig. 2A). Variability in cell density was observed between specimens and ROIs, and no significant difference was found between HER2$^-$ and HER2$^+$ specimens from cohort 1 (Fig. 2A, Suppl. Figure S3A-B). In cohort 2, comprising HER2$^+$ specimens, CD45$^+$ leukocytes were abundantly present, with a median cell density comparable to PanCK$^+$ epithelial cells (Fig. 2A, Suppl. Figure S4A-B). A greater leukocyte density was observed in cohort 2 compared to both groups in cohort 1 likely due to differences in the tissue areas available for analysis (Figs. 1C and 2A) or due to variations in specimen acquisition at different collection sites.

Paucity of NK cells in breast cancer specimens independent of HER2 status

We next investigated general leukocyte subset heterogeneity by quantifying the densities of T cells (CD45$^+$ CD3$^+$ cells), myeloid cells (CD45$^+$ CD3$^-$ CD56$^-$ NKp46$^-$ cells, identified by CD11b, CD68 or CD11c), other CD45$^+$ cells, as well as total NK cells (CD3$^-$ CD56$^+$ NKp46$^-$ cells, CD3$^-$ CD56$^+$ NKp46$^+$ cells, and CD3$^-$ CD56$^-$ NKp46$^+$ cells). Intra- and intertumoral heterogeneity was observed, and NK cells were present in low abundance (Fig. 2B, Suppl. Figure S3C-D). CD3$^+$ T cells represented the most abundant immune subset in both the HER2$^-$ and HER2$^+$ specimens in cohort 1, followed by other CD45$^+$ cells and myeloid cells with no significant differences between HER2$^-$ and HER2$^+$ disease in any of the evaluated cell populations (Fig. 2B, Suppl. Figure S3C-D). In cohort 2, CD3$^+$ T cells remained the densest immune cell population (Fig. 2B, Suppl. Figure S4C-D), consistent with previously published immune cell compositions in breast cancer cohorts [32, 33]. Further subset analysis within CD3$^+$ T cells revealed that CD4$^+$ and CD8$^+$ T cell subsets were found at comparable cell densities within both the HER2$^-$ and HER2$^+$ specimens in cohort 1 (Fig. 2C). As for total CD3$^+$ T cells, cell densities of CD4$^+$ and CD8$^+$ T cell subsets were greater in cohort 2 than in cohort 1, but CD4$^+$ and CD8$^+$ T cell densities were found at comparable ratios, which was consistent with the findings in cohort 1 (Fig. 2C). Within the myeloid cell fraction, the antibody panel allowed identification of CD11b$^-$ CD11c$^+$ and CD11b$^+$ CD11b$^-$ dendritic cells, CD11b$^+$ CD68$^+$ or CD11b$^-$ CD68$^+$ myelomonocytic cells, and other CD11b$^+$ cells, such as granulocytes; the myeloid subsets revealed

neither significant differences between HER2$^-$ and HER2$^+$ specimens in cohort 1, nor between cohorts (Fig. 2D).

The NK cell density in comparison with that of CD3$^+$ T cells and CD11b$^+$ myeloid cells is illustrated in Fig. 2E. The NK cell density ranged from 0 to 16 NK cells/mm^2 in HER2$^-$ specimens and 0–53 NK cells/mm^2 in HER2$^+$ specimens of cohort 1 (median of 8 NK cells/mm^2 in both groups, Fig. 2F, Suppl. Figure S3C-D). The cell densities of NK cells in HER2$^+$ specimens were comparable in cohort 2, where we detected 0–68 NK cells/mm^2 (median of 6.6 NK cells/mm^2, Fig. 2F, Suppl. Figure S4C-D). NK cell presence was thus not associated with HER2 status, nor with other known tumor characteristics (tumor grade, lymph node status, hormone receptors ER and PR), neoadjuvant treatment status, or CD3$^+$ or myeloid cell densities (Suppl. Table S4).

NK cells lack indicators of cytotoxicity

We next evaluated the NK cell phenotype and functional status in HER2$^-$ and HER2$^+$ specimens. Notably, the NK cell events were extremely low in some specimens, where the sum of total NK cell events from the three NK cell subsets and from all ROIs per specimen was less than 20 events in seven of the 18 specimens in cohort 1, and in three of the 30 specimens in cohort 2 (Fig. 2G). Thus, specimens with fewer than 20 events are indicated with a different color, demonstrating that they did not skew the NK cell phenotype data (Fig. 2H).

Among the assessed activating receptors and functional markers, CD16 (FcγRIIIA) was prominently expressed, although widespread CD16 expression was detected (2–88% of NK cells). The activating receptor NKG2D, the maturation marker CD57, and the functional markers Granzyme B (GRZB) and Ki67 were expressed but in a lower frequency of NK cells (average of 0–14%), indicating that tumor-infiltrating NK cells were neither highly cytotoxic nor strongly proliferative. To test whether low GRZB levels correlated with functional exhaustion, we examined NK cell positivity for TIM-3 and PD-1. Few NK cells expressed either TIM-3 (14–20%), or PD-1 (0–23% PD-1$^+$ NK cells), independent of HER2 status in the two cohorts (Fig. 2H). Overall, these results indicate that NK cells in breast cancer display a rather mature (CD16$^+$), but not terminally-differentiated nor exhausted phenotype combined with low GRZB and Ki67 expression, indicating a non-cytotoxic/proliferative profile. Of note, we observed no distinction between HER2$^-$ and HER2$^+$ specimens for any of the evaluated biomarkers.

The majority of NK cells in the tumor stroma were identified as CD56- NKp46+ NK cells

NK cells are frequently identified as CD3$^-$ CD56$^+$ or NKp46$^+$ cells owing to the majority of NK cells in the periphery expressing both CD56 (NCAM1) and the activating receptor NKp46. However, neither is sufficient alone to identify NK cells, as CD56$^-$ and NKp46$^-$ NK cell subsets have been reported [34–38]. To capture a majority of NK cells, we used both CD56 and NKp46 and identified CD56$^+$ NKp46$^-$, CD56$^-$ NKp46$^+$, and CD56$^+$ NKP46$^+$ NK cells. All three NK cell populations were found in the three specimen groups with CD56$^-$ NKp46$^+$ NK cells being the most abundant population (Fig. 2I). Interestingly, highly similar distributions of NK cell fractions were detected in both HER2$^+$ specimen groups: A trend towards a larger fraction of CD56$^+$ NKp46$^-$ NK cells observed in HER2$^+$ specimens of both cohorts compared to HER2$^-$ specimens of cohort 1, indicating that the CD56$^+$ NKp46$^-$ NK cell subset tended to correlate with HER2 status rather than with the cohorts. Further analysis for the three NK cell subsets was not performed due to low NK cell counts (Fig. 2G).

Single-cell spatial organization of NK cells revealed distinct NK cell phenotypes associated with proximity to neoplastic tumor cells and HER2 status

Although NK cells were found in low numbers in most tumor specimens, we observed that some NK cells infiltrated tumor nests, whereas other NK cells were more distal to neoplastic tumor cells, which were surrounded by other cells in the TME. An example of a tumor specimen with high NK cell counts illustrates that NK cells are distributed throughout the depicted ROI (Fig. 3A).

Since NK cells were found within PanCK$^+$ tumor nests, as well as distal to PanCK$^+$ cells, we further examined their spatial distribution and asked how NK cells inside or outside tumor nests differ. For this spatial analysis, total NK cells (CD3$^-$ CD56$^+$ NKp46$^-$ cells, CD3$^-$ CD56$^+$ NKp46$^+$ cells, and CD3$^-$ CD56$^-$ NKp46$^+$ cells) from all patients, and of both cohorts were analyzed on a single cell level. As PanCK$^+$ neoplastic epithelial cells can negatively affect NK cells, we first investigated whether proximity of the PanCK$^+$ cells to NK cells affects NK cell phenotypes. Given that NK cells are 5–10 µm and that breast cancer cells can reach ~ 30 µm, we considered a 20 µm distance for PanCK$^+$ cells to interact with NK cells and grouped them based on presence or absence of PanCK$^+$ cells within the set distance of 20 µm. Thus, NK cells were placed into the "proximal" (< 20 µm) group when at least one PanCK$^+$ cell was located within a radius of 20 µm from its cell nucleus. NK cells were placed into the "distal" (> 20 µm) group when no PanCK$^+$ cell was present within the 20 µm radius.

NK cells were detected in both spatial groups (proximal and distal) in a majority of specimens, further illustrating that not all NK cells were located outside neoplastic tumor nests but that a proportion of NK cells were located in close proximity to PanCK$^+$ neoplastic epithelial cells (Suppl. Figure S5A-C). We found that NK cells

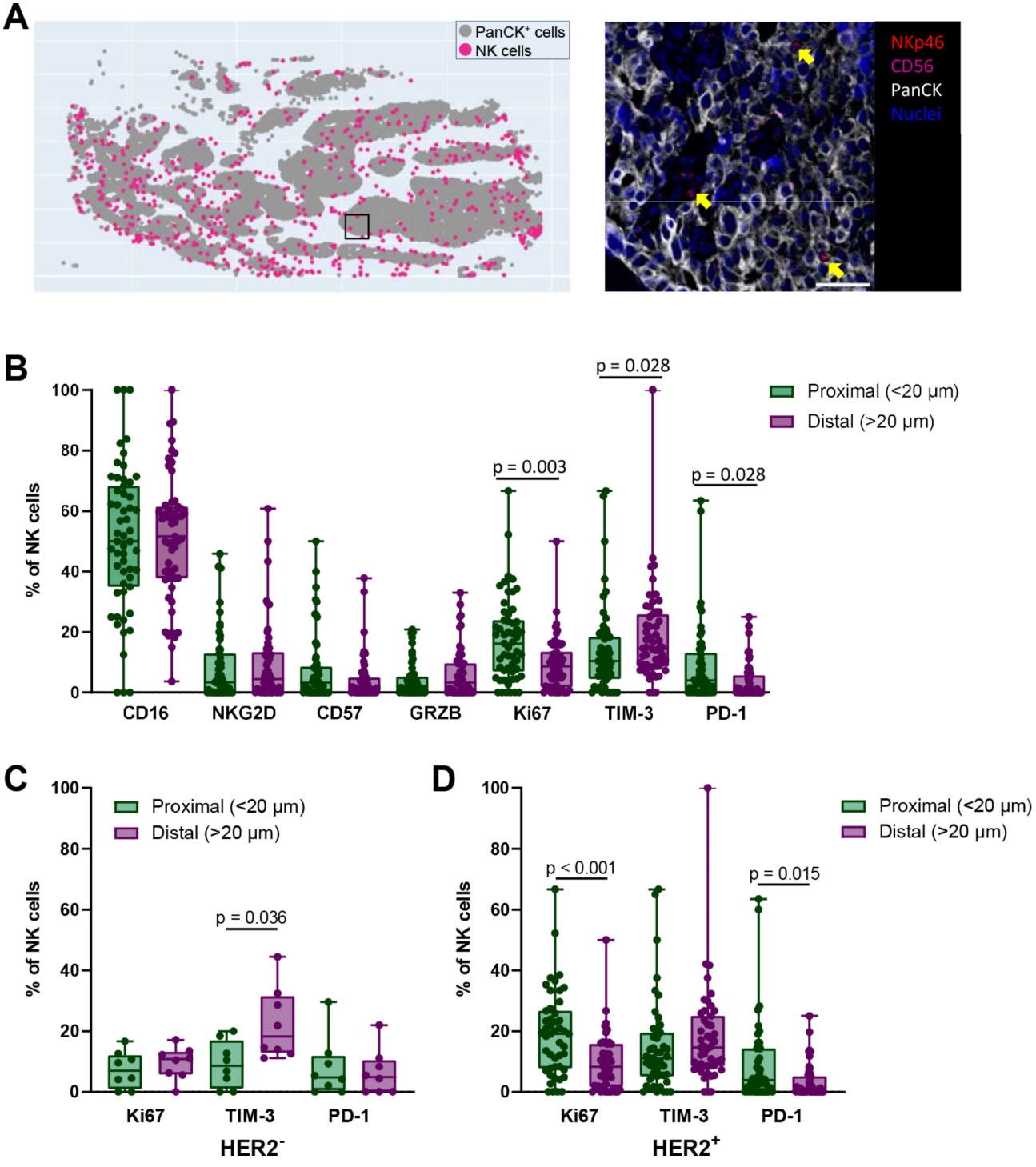

Fig. 3 Single cell analysis of NK cells results in distinct phenotypes related to the proximity to tumor cells and HER2 status. **A)** Scatterplot of a specimen with, compared to other analyzed specimens, high density of NK cells, identified by either NKp46 or CD56 (left). Pseudocolored image in higher magnification with NK cells, PanCK$^+$ cells and nuclei (Hematoxylin) with yellow arrows highlighting NK cells in tumor nests; scale bar = 50 µm (right). **B-D)** Single cell distance analysis: Each NK cell from all specimens was placed into either of the two distance groups, based on the distance threshold (20 µm) of each NK cell from PanCK$^+$ cells. Expression of phenotypic and functional markers of all NK cells, grouped as close (< 20 µm) and far (> 20 µm) from PanCK$^+$ cells (**B**). Those markers that were significantly different in (**B**) were split into HER2$^-$ specimens (**C**) and HER2$^+$ specimens (**D**). One dot represents one specimen and the % is calculated of the sum of ROIs per specimen. Boxes represent Q1-Q3 with the line showing the mean and whiskers the smallest and largest data point within the quartile range

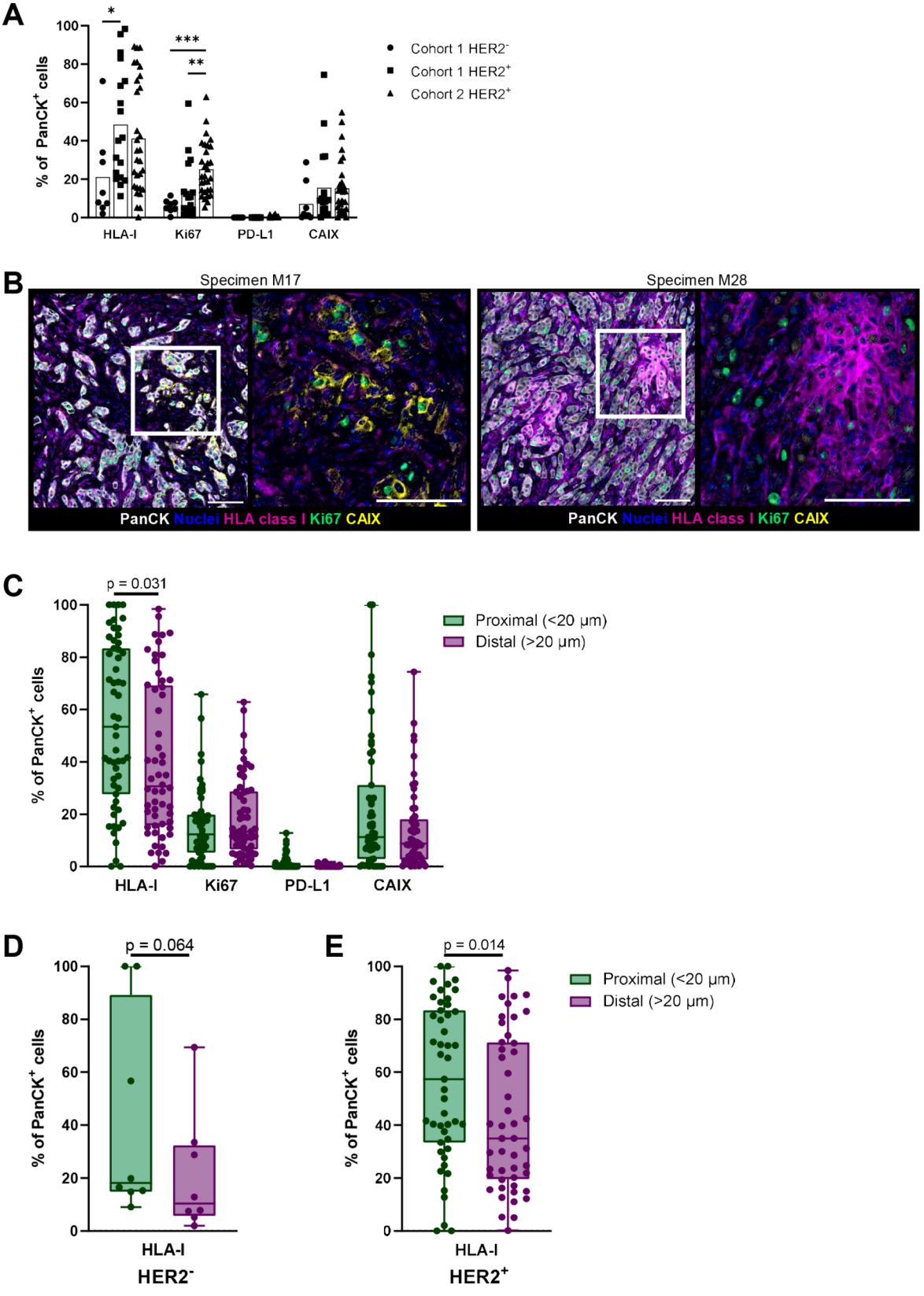

Fig. 4 (See legend on next page.)

(See figure on previous page.)

Fig. 4 Single-cell analysis of neoplastic PanCK$^+$ epithelial cells illustrate heterogeneity and high HLA class I expression close to NK cells. **(A)** Expression of phenotypic markers on PanCK$^+$ cells. **(B)** Pseudocolored images showing two examples with heterogeneous staining patterns of HLA class I, Ki67, and CAIX in combination with nuclear staining (Hematoxylin). Higher magnification is displayed on the right without PanCK. Scale bars = 100 µm. **C-E)** Distance analysis: PanCK$^+$ cells were placed into either of the two groups based on the distance threshold (20 µm) of each PanCK$^+$ cells from NK cells. Expression of phenotypic markers of all PanCK$^+$ cells, grouped as proximal (< 20 µm) or distal (> 20 µm) from NK cells (**C**). Significantly different HLA-I expression was split into HER2$^-$ specimens (**D**) and HER2$^+$ specimens (**E**). One dot represents one specimen and the % is calculated as sum of ROIs per specimen. Boxes represent Q1-Q3 with the line showing the mean and whiskers the smallest and largest data point

close to PanCK$^+$ cells tended to be Ki67$^+$, reflecting their proliferative status, and expressed the checkpoint molecule PD-1, but fewer expressed TIM-3 (Fig. 3B).

We next questioned whether differences in expression of functional indicators on NK cells proximal or distal to PanCK$^+$ cells related to HER2 status. We split NK cells based on HER2 status of the original specimen where NK cells were identified and assessed the functional status of the two NK cell spatial groups (proximal and distal) separately. Interestingly, increased numbers of NK cells expressing both Ki67 and PD-1 proximal to PanCK$^+$ cells were observed in HER2$^+$ specimens (Fig. 3C-D). Moreover, an increased density of NK cells expressing TIM-3 was observed in cells distal to PanCK$^+$ cells in HER2$^-$ specimens, whereas the difference trended in HER2$^+$ specimens (Fig. 3C-D). Although the modest sample size for the HER2$^-$ group limited definitive conclusion, these findings do reveal that NK cells localizing inside and outside tumor nests are phenotypically distinct, and may be additionally related to HER2 status. To further investigate the impact of proximal neoplastic tumor cells to NK cells, we subsequently interrogated the neoplastic tumor cell phenotype and leukocyte composition correlating with spatial proximity to NK cells.

PanCK+ neoplastic cells exhibit extensive heterogeneity and retain high HLA class I expression when in close proximity to NK cells

Because the phenotype of PanCK$^+$ neoplastic cells may influence susceptibility to NK cell-mediated killing, we evaluated HLA class I expression as a major inhibitory ligand for NK cells, cell proliferation (Ki67), the immune checkpoint ligand PD-L1 and hypoxia (carbonic anhydrase IX, CAIX) on PanCK$^+$ neoplastic cells (Fig. 4A). We observed large variations in HLA-I expression between the individual tumor specimens in all three specimen groups, with slightly increased HLA class I-positive PanCK$^+$ cells in HER2$^+$ specimens (Fig. 4A-B). Proliferation of PanCK$^+$ neoplastic cells was observed in a small fraction of cells in HER2$^-$ specimens (average of 6%). In comparison, higher densities of Ki67$^+$ neoplastic cells were observed in both HER2$^+$ groups (average of 14% cohort 1 and 25% cohort 2), but without significant differences between HER2$^-$ and HER2$^+$ specimens in cohort 1. The percentage of CAIX$^+$ neoplastic cells varied between specimens, and hypoxic areas were detected in a majority of specimens, independent of HER2 status. PD-L1 expression was not observed on the PanCK$^+$ cells in any of the conditions, indicating that the PD-1$^+$ NK cells are likely not inhibited through epithelial PD-L1 (Fig. 4A).

Since close contact between NK cells and their target cells is crucial for NK cell-mediated killing, we subsequently asked how tumor cell phenotypes differed with regards to NK cell proximity (Fig. 4C). Using the same distance threshold of 20 µm as for NK cells, each single PanCK$^+$ tumor cell was placed either in the "proximal" (< 20 µm) group when at least one NK cell was located within a 20 µm radius, or they were placed in the "distal" (> 20 µm) group when no NK cells were within 20 µm. Although HLA-I expression was highly heterogenous in both groups, the analysis revealed a significantly higher percentage of HLA-I expressing PanCK$^+$ cells proximal to NK cells (Fig. 4C). The expression of Ki67, PD-L1, and CAIX-positive cells was not significantly different between neoplastic tumor cells proximal or distal to NK cells.

Based on the observations of increased presence of HLA class I-expressing cells in HER2$^+$ specimens, and that these tended to be proximally located to NK cells, we evaluated the difference in HLA-I$^+$ cells to NK cells based on HER2 status directly. The number of HLA-I$^+$ neoplastic cells proximal to NK cells tended to increase in HER2$^-$ specimens (Fig. 4D) but was significantly higher in HER2$^+$ specimens (Fig. 4E). Although a larger fraction of PanCK$^+$ neoplastic cells expressed HLA-I within the HER2$^+$ cohort, neoplastic cells close to NK cells expressed HLA-I in higher fractions in both cohorts. These results indicate that HLA-I expression on neoplastic tumor cells is related to spatial proximity of NK cells, and may be impacted by HER2 status. As HLA-I molecules are major inhibitory ligands for NK cells, our finding of HLA-I$^+$ tumor cells close to NK cells supports that HLA-I expression may be a mechanism by which breast cancer cells escape NK cell-mediated killing.

NK cells reside in distinct spatial cellular neighborhoods, which are associated with HER2 biology

Having analyzed the pairwise interactions between NK cells and neoplastic epithelial cells, we sought to identify cells surrounding NK cells beyond 20 µm, to include neoplastic cells as well as other leukocyte subsets. Thus, we performed a cellular neighborhood analysis and set the distance threshold to 60 µm allowing for inclusion of cells close enough to directly touch NK cells, and also

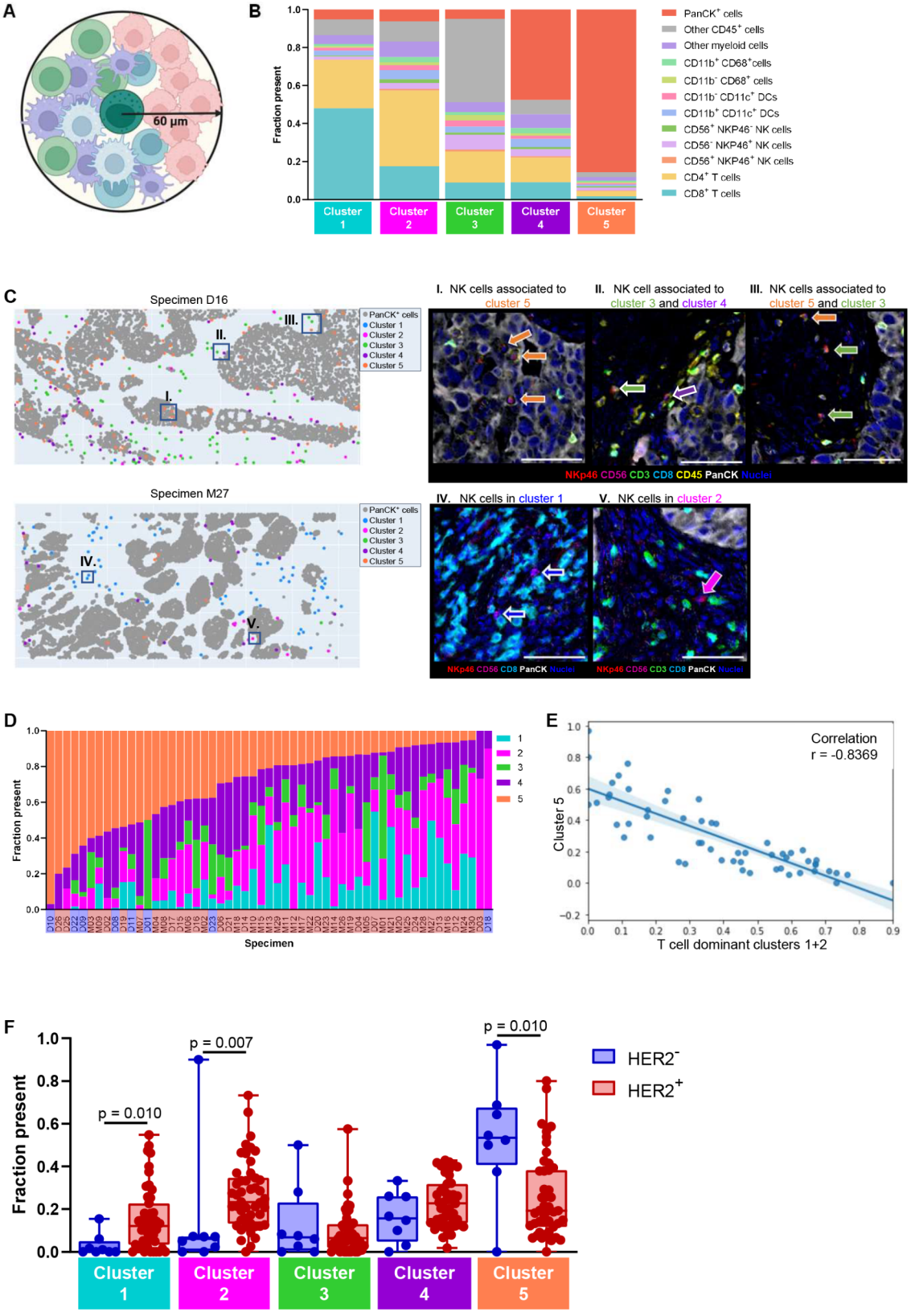

Fig. 5 (See legend on next page.)

(See figure on previous page.)

Fig. 5 Cellular neighborhood clustering of NK cells. **(A)** Cellular neighborhood definition. A circle of 60 µm radius was drawn around each NK cell, identified by either NKp46 or CD56. The cells inside the circle were counted as neighbors of NK cells. **(B)** All specimens were pooled and analyzed for NK cell neighborhood clusters. The average cellular composition of each of the five NK cell neighborhood clusters is shown. **(C)** Left: Scatterplots of two specimens with comparatively high NK cell counts to illustrate the distribution of the NK cell neighborhoods clusters. PanCK$^+$ cells are shown in grey together with all NK cells, which are colored by the cluster they were assigned to. Right: Corresponding pseudocolored mIHC images of each NK cell neighborhood cluster. Scale bars = 60 µm. **(D)** The average proportion of each NK cell neighborhood cluster is shown for each patient, except for one patient of cohort 1, in which no NK cells were detected. Specimens are sorted by proportions of cluster 5 and color of specimen ID represents HER2 status (HER2$^-$ in blue, HER2$^+$ in red). **(E)** Negative correlation of the T cell dominant clusters 1 and 2 and the tumor dominant cluster 5. **(F)** Cellular composition of the NK cell neighborhood clusters for HER2$^-$ and HER2$^+$ specimens of both cohorts

accounting for neighboring cells interacting with NK cells through cytokine signaling (Fig. 5A) [39, 40]. All NK cells, identified by either CD56 or NKp46 expression, were considered for this analysis. Any NK cell that did not have a neighbor within the distance threshold was removed from downstream analyses. After the cellular neighborhoods were calculated, k-means clustering was used to group the neighborhoods into five clusters, each with unique cellular compositions (Fig. 5B). On average, neighborhoods assigned to cluster 1 and cluster 2 consisted mainly of T cells; cluster 1 neighborhoods were dominated by CD8$^+$ T cells (representing ~ 50% of the cellular makeup), whereas cluster 2 neighborhoods were characterized by a majority of CD4$^+$ T cells as neighboring cells. Cluster 3 neighborhoods were mainly defined by other CD45$^+$ leukocytes, not further characterized in this study. Neighborhoods in clusters 4 and 5 were predominantly PanCK$^+$ neoplastic cells, although differing in proportion. Cluster 4 neighborhoods represented a mixture of neoplastic tumor cells and immune cell subsets, whereas Cluster 5 neighborhoods contained the largest proportion of neoplastic tumor cells (> 80% of neighbors). No cluster was dominated by NK cells, and NK cells were rarely found neighboring each other, but instead distributed across tissue regions. Despite this broad spatial localization of NK cells across a given region, NK cells localized in the T cell dominant neighborhood clusters 1 and 2 were often found outside of tumor nests, whereas NK cells in the tumor-immune cluster 4 were predominantly observed at the tumor-stroma border (Fig. 5C).

The distribution of neighborhood clusters revealed that no single cluster was dominant and that all five clusters were represented in comparable proportions (Suppl. Figure S7A). Moreover, most clusters were present in every specimen (Fig. 5D) and in every ROI (Suppl. Figure S7B), thus indicating that no cluster was driven by the spatial organization of a single tumor or region. Interestingly, we observed a negative correlation between the presence of the neoplastic tumor dominant neighborhood cluster 5 and the T cell dominant neighborhood clusters 1 and 2 (Fig. 5D-E). This finding indicates that NK cells are unlikely to have both neoplastic tumor cells and T cells as neighbors. Other cluster combinations did not correlate (data not shown). The cellular densities of NK cells were not strongly correlated with densities of other identified immune cell types (Suppl. Fig. S6), supporting the notion that the described neighborhood clusters are a result of the cellular spatial organization and that the neighborhood clusters are not driven by just the mere presence of the identified immune cell types.

Finally, we examined whether the proportion of NK cells assigned to each of the neighborhood clusters varied between HER2$^-$ and HER2$^+$ patients. Significant differences were observed for the CD8$^+$ T cell dominant cluster 1, the CD4$^+$ T cell dominant cluster 2, and the PanCK$^+$ tumor cell-dominant cluster 5 (Fig. 5F). A larger fraction of NK cells was attributed to neighborhood cluster 5 in HER2$^-$ patients than in HER2$^+$ patients, indicating that NK cells in HER2$^-$ patients were more common near neoplastic tumor cells. In HER2$^+$ patients, we observed a higher fraction of NK cells within the two T cell-dominant clusters (Cluster 1 and 2), implying that the NK cells in HER2$^+$ patients were more often surrounded by CD8$^+$ and CD4$^+$ T cells than were the NK cells in HER2$^-$ patients. As we detected a higher density of CD3$^+$ T cells in cohort 2 than in cohort 1, we repeated the comparison of HER2 status using only cohort 1 patients and found the same trends (Suppl. Figure S7C), supporting the notion that NK cell spatial neighbors may be related to HER2 status.

Overall, we revealed that distinct cellular neighborhoods surrounding NK cells exist in human breast cancer. Each neighborhood contained unique compositions, with NK cells localizing more frequently in the tumor-dominant neighborhood cluster in the HER2$^-$ specimens, whereas NK cells localized in the two T cell-dominant neighborhood clusters more often in the HER2$^+$ specimens (Fig. 6). Altogether, these results suggest to consider the spatial architecture of TME cells surrounding NK cells when planning breast cancer therapy. Based on our results, we further hypothesize that immunotherapies leveraging the coordinated anti-tumor function of both NK cells and T cells may be beneficial for HER2$^+$ patients especially, given the spatial proximity of T cells to NK cells in these specimens.

Discussion

An improved understanding of NK cells and their spatial distribution in the TME of breast cancer can guide future design of successful NK cell-based immunotherapies.

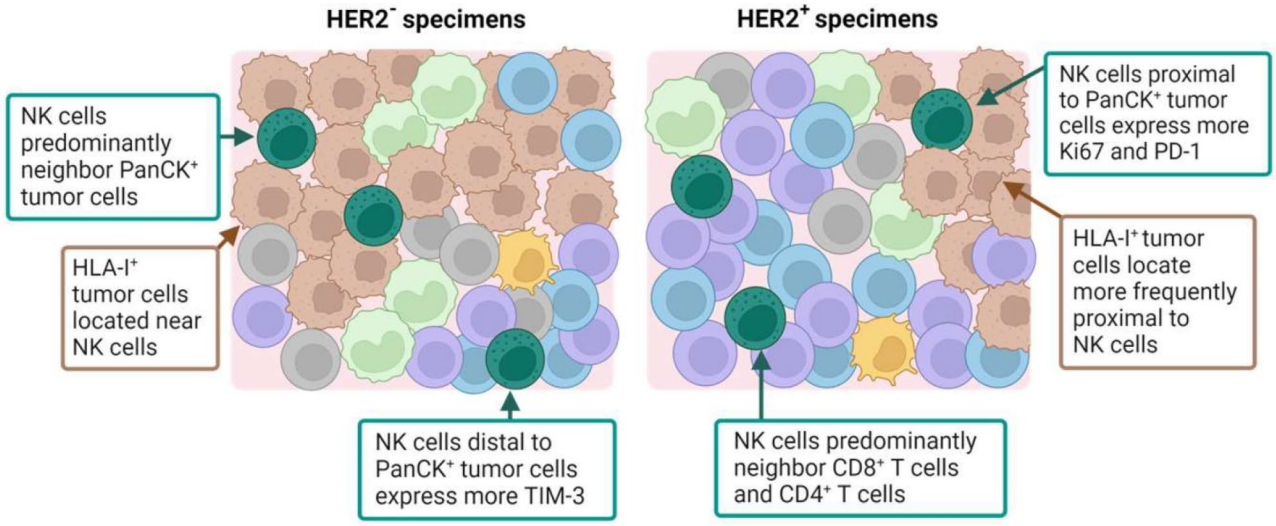

Fig. 6 NK cells reside in unique spatial niches in the tumor microenvironments of human breast cancer. Depicted are the significantly different findings for NK cell localization and phenotype, associated with HER2 status in this study

In this study, we developed an mIHC panel focused on NK cells to evaluate density, phenotype and spatial organization in relation to neoplastic tumor cells and other tumor-infiltrating leukocytes. The mIHC methodology enabled quantification of immune cell populations and phenotypes at the single-cell level, while maintaining tissue spatial architecture. In this study, $CD3^+$ T cells were by far the most dominant leukocyte present in all analyzed groups with immune cell contexture largely comparable with the immune cell compositions reported previously in breast cancer by flow cytometry analysis [32, 33, 41].

Results herein indicate that in two breast cancer cohorts where HER2 status was known, NK cell density was not found to correlate with HER2 status, or with other parameters including neoadjuvant treatment or ER/PR status. In a different study, we did observe that in polyclonal metastatic breast cancer adjuvant therapy significantly impacts both immune contexture and state [27]. Based on those results, and published reports [42, 43], we anticipate that neoadjuvant therapy similarly would be impactful, but based on cohort size, we were not able to include that parameter herein. That said, hormone receptor-positive breast cancers tend to be less infiltrated by immune cells as compared to triple-negative and $HER2^+$ subtypes [44]. Similarly, ER expression is reported to negatively correlate with NK cell presence where higher NK cell densities were detected in ER^- tumors as compared to ER^+ tumors [45, 46], underlining that association with HER2 status alone as performed in the present study is likely not the only tumor feature impacting NK cell localization in human breast cancer [44].

To detect NK cells, we evaluated the expression of CD56 and the activating receptor NKp46 and found that the majority of NK cells expressed both, consistent with a report describing that NKp46 was largely retained in several solid tumors [47]. The activating receptor CD16, generally expressed on mature $CD56^{dim}$ NK cells, was expressed on all specimens except two, but with rather low frequency in some. Identification of both $CD16^+$ and $CD16^-$ NK cells inside tumors has been reported previously [47, 48]. Preferred recruitment of $CD16^-$ $CD56^{bright}$ NK cells to breast tissues might be one possibility for the observed heterogeneous CD16 expression on tumor-infiltrating NK cells [9]. Alternatively, the receptor can be cleaved by metalloproteases following NK cell activation [49]. The heterogeneous expression of CD16 could have consequences for effectiveness of ADCC-mediating antibodies since CD16 levels were reported to positively correlate with the potency of ADCC [50]; and for therapeutic purposes, the underlying mechanism of heterogeneous CD16 expression should be unraveled. Further, NK cells were not terminally differentiated in this study based on low detection of CD57. It was reported that $CD57^+$ NK cells were reduced in breast cancer tissue compared to peripheral blood, indicating limited homing to tumor or decreased survival of $CD57^+$ tumor-infiltrating NK cells [51]. Moreover, NK cells in the cohorts evaluated herein did not abundantly express GRZB and Ki67, indicating a lack of cytotoxicity and proliferative capacity. Our image analysis approach detected GRZB expression when the signal was associated with the cell; GRZB could therefore have been released into the TME before tumor tissue resection. Alternatively, NK cells could be non-cytotoxic as a consequence of the immunosuppressive TME in breast cancer. Accordingly, various NK cell subsets have

been identified in recent pan-cancer RNA-sequencing studies, including non-cytotoxic NK cells susceptible to immunosuppression [52, 53]. The NKp46$^+$ NK cells may also belong to the group of non-cytotoxic innate lymphoid cells type 1 (ILC1) [54]. The conversion of NK cells to ILC1 has been reported as a tumor immune evasion strategy, although functions of ILC1 are highly variable, depending on the cytokines present in the TME [54, 55]. Additional makers would be required to distinguish NK cell subsets and ILCs in our study.

Previous studies also reported that NK cells can be confined to tumor stroma rather than infiltrating neoplastic cell nests [56, 57]. We observed that NK cells were located either "proximal" (< 20 µm) or "distal" to neoplastic tumor cells (> 20 µm). Higher densities of proliferating and PD-1$^+$ NK cells, and fewer expressing TIM-3 "proximal" to PanCK$^+$ cells as compared to NK cells "distal" to PanCK$^+$ neoplastic cells indicate the likelihood that the TME shapes NK cell phenotype and spatial organization. On PanCK$^+$ neoplastic cells, we found not only HLA class I expression with large intertumoral heterogeneity, in line with previous publications [58, 59], but also increased presence of HLA class I-expressing cells close to NK cells. This finding indicates that neoplastic tumor cells may retain HLA class I expression in areas where NK cells are localized, potentially as an immune escape mechanism. Our observation provides rationale for interfering with HLA class I-mediated inhibition e.g., by selecting donor NK cells lacking the corresponding KIR receptor for the HLA type expressed by breast tumors (KIR-HLA ligand mismatched NK cells). Alternatively, sufficient NK cell activating signals must be provided to overcome HLA-mediated inhibition. Given the low abundance of NK cells in many solid tumors, as observed herein, therapeutic innovations targeting NK cells generally include strategies to enhance NK cell numbers, e.g. by cytokine stimulation, ex vivo expansion, or strategies to enhance migration and/or survival of NK cells in the TME, e.g. by multispecific NK cell engagers and/or genetic modification of NK cells, aiming to overcome TME resistance mechanisms [15, 60]. Similar to the heterogeneous HLA-I expression, heterogeneous CAIX expression indicated that hypoxia occurred in local areas of all tumor tissues examined. The result that NK cells close to neoplastic tumor cells were not associated with higher CAIX expression indicates that NK cells can infiltrate independently of hypoxia. However, NK cell functions are known to be influenced negatively by the presence of hypoxia and should therefore be considered for NK cell-targeting therapies [61]. PD-L1 expression was not detected on PanCK$^+$ cells, in agreement with published data showing that PD-L1 expression on neoplastic tumor cells was not a prominent feature of human breast cancer [62, 63].

We further set out to understand the cellular spatial organization surrounding NK cells, beyond directly adjacent neoplastic tumor cells, and identified five distinct NK cell neighborhood clusters. Most strikingly was the observed negative correlation between NK cell neighborhoods consisting of predominately CD3$^+$ T cells (cluster 1 and 2) and the neoplastic tumor neighborhood (cluster 5) indicating that NK cells are predominantly surrounded by neoplastic tumor cells or T cells but not both, thus a tumor feature in need of consideration for either NK cell- or other immune cell-based immune therapy. In breast cancers where NK cells reside close to neoplastic cells, this feature trended more with HER2$^-$ tumors, thus NK cell-engaging molecules that promote direct cytotoxic function (e.g. immune checkpoint blockade and enhancing ADCC) may be beneficial, whereas in breast cancers with NK cells near T cells, a potential therapeutic approach could aim to stimulate cytokine production by NK cells to subsequently orchestrate an adaptive T cell-mediated immune response. Our findings support the conclusions by Namara et al., that reported NK cells mostly reside in tumor areas, while T cells predominantly reside in surrounding TME of treatment-naive breast cancer [64]. Supporting this, a study in HER2$^+$ disease where patients received Trastuzumab reported that both NK cells and T cells are major contributors to observed anti-tumor responses [14]. Since NK cells and T cells are both cytotoxic effector cells, future studies may aim to interrogate the spatial distribution from the perspective of T cells.

In conclusion, spatial analyses reported herein reveal that NK cells occupy unique spatial neighborhoods in breast cancer microenvironments. While correlations of NK cell spatial organization with HER2 status are based upon evaluation of over 10,000 NK cells, the number of HER2$^-$ specimens ($n = 8$) in the present study was low. Thus, future studies will need to evaluate larger patient cohorts with equal group sizes to validate our current findings. Despite this limitation, this study provides an in-depth analysis of NK cells in relation to surrounding neoplastic tumor cells and leukocyte subsets in HER2$^+$ and HER2$^-$ breast cancer. Upon additional validation in larger cohorts, the spatial architecture of NK cells in the TME may be a feature to consider for patient stratification or for design of NK cell-targeted therapeutic innovations tailored to HER2$^-$ or HER2$^+$ breast cancer.

Supplementary Information

The online version contains supplementary material available at https://doi.org/10.1186/s13058-025-01964-4.

Supplementary Material 1

Acknowledgements
We thank the mIHC team of the Coussens laboratory for their assistance. F.A.I. Ehlers is grateful for the support by a TEFAF fellowship, awarded by GROW - School for Oncology and Reproduction, Maastricht University.

Author contributions
Conceptualization and design of the study, F.A.I.E., C.B.B, G.M.J.B., L.W., L.M.C.; Investigation, F.A.I.E., K.E.B, S.S.; Data generation and analysis, F.A.I.E. , K.E.B., S.S., C.B.; Ressources, L.F.S.K., E.S.H.; Writing—original draft preparation, F.A.I.E., K.E.B., S.S., L.M.C.; Writing—review and editing, C.B.B, L.F.S.K., E.S.H., L.W., L.M.C.; Supervision, G.M.J.B., L.W., L.M.C. All authors read, reviewed, and approved the manuscript.

Funding
G.M.J. Bos and L. Wieten received support from Kankeronderzoeksfonds Limburg (KOFL). K.E. Blise acknowledges funding from the National Cancer Institute (NCI) of the National Institutes of Health under award number T32CA254888. E. S. Hwang received funding from NIH/NCI (U2CCA233254-01, R01CA222508) and acknowledges support from the Susan G Komen Foundation. L.M. Coussens acknowledges support from the Susan G Komen Foundation, the National Foundation for Cancer Research, and the Knight Cancer Institute at OHSU.

Data availability
The mIHC data used for this study is available for download on Zenodo at https://doi.org/10.5281/zenodo.10632694. The code used to generate the spatial results of this study was created using Python version 3.9.4 and is available on Github at https://github.com/kblise/NKcell_mIHC_paper.

Declarations

Ethics approval
Cohort 1 samples were obtained from Duke University, Durham, USA. Informed consent was obtained from all human subjects included in this study. The study protocol was approved by the ethics committee IRB of Duke University (Pro00034242). Cohort 2 samples were obtained by Maastricht University Medical Center+, Maastricht, The Netherlands. The collection, storage, and use of tissue and patient data were performed in agreement with the "Code for Proper Secondary Use of Human Tissue in the Netherlands" and approved by the local ethics committee (METC 2019 – 1154).

Consent for publication
Not applicable.

Conflict of interest
C.B. Betts is an employee of, and holds equity in, Akoya Biosciences, Inc. L.M. Coussens has received reagent support from Cell Signaling Technologies, Syndax Pharmaceuticals, Inc., ZielBio, Inc., and Hibercell, Inc.; holds sponsored research agreements with Syndax Pharmaceuticals, Hibercell, Inc., Prospect Creek Foundation, Lustgarten Foundation for Pancreatic Cancer Research, Susan G. Komen Foundation and the National Foundation for Cancer Research; is on the Advisory Board for Carisma Therapeutics, Inc., CytomX Therapeutics, Inc., Kineta, Inc., Hibercell, Inc., Cell Signaling Technologies, Inc., Alkermes, Inc., Raska Pharma, Inc., NextCure, Guardian Bio, AstraZeneca Partner of Choice Network (OHSU Site Leader), Genenta Sciences, Pio Therapeutics Pty Ltd., and Lustgarten Foundation for Pancreatic Cancer Research Therapeutics Working Group, Inc.

Author details
[1]Department of Transplantation Immunology, Tissue Typing Laboratory, Maastricht University Medical Center+, Maastricht 6229, HX, The Netherlands
[2]Department of Internal Medicine, Division of Hematology, Maastricht University Medical Center+, Maastricht 6229 HX, The Netherlands
[3]GROW - School for Oncology and Reproduction, Maastricht University, Maastricht 6229 GT, The Netherlands
[4]Department of Biomedical Engineering, Oregon Health & Science University, Portland, OR 97239, USA
[5]Department of Cell, Developmental & Cancer Biology, Oregon Health & Science University, Portland, OR 97239, USA
[6]Department of Pathology, Maastricht University Medical Center+, Maastricht 6229 HX, The Netherlands
[7]Department of Surgery, Duke University Medical Center, Durham, NC 27710, USA
[8]Knight Cancer Institute, Oregon Health & Science University, Portland, OR 97239, USA
[9]2720 S Moody Ave, #KC-CDCB, Portland, OR 97201 – 5012, USA

Received: 25 August 2024 / Accepted: 12 January 2025
Published online: 24 January 2025

References

1. Sung H, Ferlay J, Siegel RL, Laversanne M, Soerjomataram I, Jemal A, Bray F. Global cancer statistics 2020: GLOBOCAN estimates of incidence and mortality worldwide for 36 cancers in 185 countries. CA Cancer J Clin. 2021;71:209–49.
2. Rivenbark AG, O'Connor SM, Coleman WB. Molecular and cellular heterogeneity in breast cancer: challenges for personalized medicine. Am J Pathol. 2013;183:1113–24.
3. Savas P, Salgado R, Denkert C, Sotiriou C, Darcy PK, Smyth MJ, Loi S. Clinical relevance of host immunity in breast cancer: from TILs to the clinic. Nat Reviews Clin Oncol. 2016;13:228–41.
4. Wang W, Erbe AK, Hank JA, Morris ZS, Sondel PM. NK cell-mediated antibody-dependent cellular cytotoxicity in cancer immunotherapy. Front Immunol. 2015;6:368.
5. Bryceson YT, March ME, Ljunggren H-G, Long EO. Synergy among receptors on resting NK cells for the activation of natural cytotoxicity and cytokine secretion. Blood. 2006;107:159–66.
6. Vivier E, Tomasello E, Baratin M, Walzer T, Ugolini S. Functions of natural killer cells. Nat Immunol. 2008;9:503–10.
7. Barry KC, Hsu J, Broz ML, Cueto FJ, Binnewies M, Combes AJ, Nelson AE, Loo K, Kumar R, Rosenblum MD. A natural killer–dendritic cell axis defines checkpoint therapy–responsive tumor microenvironments. Nat Med. 2018;24:1178–91.
8. Melaiu O, Lucarini V, Cifaldi L, Fruci D. Influence of the tumor microenvironment on NK cell function in solid tumors. Front Immunol. 2020;10:3038.
9. Bald T, Krummel MF, Smyth MJ, Barry KC. The NK cell–cancer cycle: advances and new challenges in NK cell–based immunotherapies. Nat Immunol. 2020;21:835–47.
10. Clynes RA, Towers TL, Presta LG, Ravetch JV. Inhibitory fc receptors modulate in vivo cytoxicity against tumor targets. Nat Med. 2000;6:443–6.
11. Park S, Jiang Z, Mortenson ED, Deng L, Radkevich-Brown O, Yang X, Sattar H, Wang Y, Brown NK, Greene M. The therapeutic effect of anti-HER2/neu antibody depends on both innate and adaptive immunity. Cancer Cell. 2010;18:160–70.
12. Arnould L, Gelly M, Penault-Llorca F, Benoit L, Bonnetain F, Migeon C, Cabaret V, Fermeaux V, Bertheau P, Garnier J. Trastuzumab-based treatment of HER2-positive breast cancer: an antibody-dependent cellular cytotoxicity mechanism? Br J Cancer. 2006;94:259–67.
13. Beano A, Signorino E, Evangelista A, Brusa D, Mistrangelo M, Polimeni MA, Spadi R, Donadio M, Ciuffreda L, Matera L. Correlation between NK function and response to trastuzumab in metastatic breast cancer patients. J Transl Med. 2008;6:1–10.
14. Muntasell A, Rojo F, Servitja S, Rubio-Perez C, Cabo M, Tamborero D, Costa-García M, Martínez-Garcia M, Menéndez S, Vazquez. I. NK cell infiltrates and HLA class I expression in primary HER2 + breast cancer predict and uncouple pathological response and disease-free survival. Clin Cancer Res. 2019;25:1535–45.
15. Myers JA, Miller JS. Exploring the NK cell platform for cancer immunotherapy. Nat Reviews Clin Oncol. 2021;18:85–100.
16. Fuentes-Antras J, Guevara-Hoyer K, Baliu-Piqué M, García-Sáenz JAn.;, Pérez-Segura P, Pandiella A, Ocaña A Adoptive cell therapy in breast cancer, editors. a current perspective of next-generation medicine. *Front. Oncol.* 2020, 2376.
17. Long EO, Sik Kim H, Liu D, Peterson ME, Rajagopalan S. Controlling natural killer cell responses: integration of signals for activation and inhibition. Annu Rev Immunol. 2013;31:227–58.
18. Cózar B, Greppi M, Carpentier S, Narni-Mancinelli E, Chiossone L, Vivier E. Tumor-infiltrating natural killer cells. Cancer Discov. 2021;11:34–44.
19. Tan E, Yan M, Campo L, Han C, Takano E, Turley H, Candiloro I, Pezzella F, Gatter K, Millar E. The key hypoxia regulated gene CAIX is upregulated in

basal-like breast tumours and is associated with resistance to chemotherapy. Br J Cancer. 2009;100:405–11.
20. Mamessier E, Sylvain A, Bertucci F, Castellano R, Finetti P, Houvenaeghel G, Charaffe-Jaufret E, Birnbaum D, Moretta A, Olive D. Human breast tumor cells induce self-tolerance mechanisms to avoid NKG2D-mediated and DNAM-mediated NK cell recognition. Cancer Res. 2011;71:6621–32.
21. Mamessier E, Sylvain A, Thibult M-L, Houvenaeghel G, Jacquemier J, Castellano R, Gonçalves A, André P, Romagné F, Thibault G. Human breast cancer cells enhance self tolerance by promoting evasion from NK cell antitumor immunity. J Clin Investig. 2011;121:3609–22.
22. Ehlers FA, Beelen NA, van Gelder M, Evers TM, Smidt ML, Kooreman LF, Bos GM, Wieten L. ADCC-Inducing antibody trastuzumab and selection of KIR-HLA ligand mismatched donors enhance the NK Cell Anti-breast Cancer Response. Cancers (Basel). 2021;13:3232.
23. Wilson BE, Gorrini C, Cescon DW. Breast cancer immune microenvironment: from pre-clinical models to clinical therapies. Breast Cancer Res Treat 2021, 1–11.
24. Keren L, Bosse M, Marquez D, Angoshtari R, Jain S, Varma S, Yang S-R, Kurian A, Van Valen D, West R. A structured tumor-immune microenvironment in triple negative breast cancer revealed by multiplexed ion beam imaging. *Cell* 2018, *174*, 1373–1387. e1319.
25. Tsujikawa T, Kumar S, Borkar RN, Azimi V, Thibault G, Chang YH, Balter A, Kawashima R, Choe G, Sauer D. Quantitative multiplex immunohistochemistry reveals myeloid-inflamed tumor-immune complexity associated with poor prognosis. Cell Rep. 2017;19:203–17.
26. Banik G, Betts CB, Liudahl SM, Sivagnanam S, Kawashima R, Cotechini T, Larson W, Goecks J, Pai SI, Clayburgh DR. High-dimensional multiplexed immunohistochemical characterization of immune contexture in human cancers. In *Methods Enzymol.*; Elsevier: 2020; Volume 635, pp. 1–20.
27. Johnson BE, Creason AL, Stommel JM, Keck JM, Parmar S, Betts CB, Blucher A, Boniface C, Bucher E, Burlingame E. An omic and multidimensional spatial atlas from serial biopsies of an evolving metastatic breast cancer. Cell Rep Med 2022, *3*.
28. Tsujikawa T, Mitsuda J, Ogi H, Miyagawa-Hayashino A, Konishi E, Itoh K, Hirano S. Prognostic significance of spatial immune profiles in human solid cancers. Cancer Sci. 2020;111:3426–34.
29. Sorrelle N, Ganguly D, Dominguez AT, Zhang Y, Huang H, Dahal LN, Burton N, Ziemys A, Brekken RA. Improved multiplex immunohistochemistry for immune microenvironment evaluation of mouse formalin-fixed, paraffin-embedded tissues. J Immunol. 2019;202:292–9.
30. Liudahl SM, Betts CB, Sivagnanam S, Morales-Oyarvide V, Da Silva A, Yuan C, Hwang S, Grossblatt-Wait A, Leis KR, Larson W. Leukocyte heterogeneity in pancreatic ductal adenocarcinoma: phenotypic and spatial features associated with clinical outcome. Cancer Discov. 2021;11:2014–31.
31. Blise KE, Sivagnanam S, Banik GL, Coussens LM, Goecks J. Single-cell spatial architectures associated with clinical outcome in head and neck squamous cell carcinoma. NPJ Precision Oncol. 2022;6:10.
32. Ruffell B, Au A, Rugo HS, Esserman LJ, Hwang ES, Coussens LM. Leukocyte composition of human breast cancer. Proc Natl Acad Sci. 2012;109:2796–801.
33. Del Alcazar CRG, Huh SJ, Ekram MB, Trinh A, Liu LL, Beca F, Zi X, Kwak M, Bergholtz H, Su Y. Immune escape in breast cancer during in situ to invasive carcinoma transition. Cancer Discov. 2017;7:1098–115.
34. Mamessier E, Pradel LC, Thibult M-L, Drevet C, Zouine A, Jacquemier J, Houvenaeghel G, Bertucci F, Birnbaum D, Olive D. Peripheral blood NK cells from breast cancer patients are tumor-induced composite subsets. J Immunol. 2013;190:2424–36.
35. Mahgoub S, Abosalem H, Emara M, Kotb N, Maged A, Soror S. Restoring NK cells functionality via cytokine activation enhances cetuximab-mediated NK-cell ADCC: a promising therapeutic tool for HCC patients. Mol Immunol. 2021;137:221–7.
36. Chretien A-S, Devillier R, Granjeaud S, Cordier C, Demerle C, Salem N, Wlosik J, Orlanducci F, Gorvel L, Fattori S. High-dimensional mass cytometry analysis of NK cell alterations in AML identifies a subgroup with adverse clinical outcome. *Proceedings of the National Academy of Sciences* 2021, *118*.
37. Garcia-Iglesias T, del Toro-Arreola A, Albarran-Somoza B, del Toro-Arreola S, Sanchez-Hernandez PE, Ramirez-Dueñas MG, Balderas-Peña LM, Bravo-Cuellar A, Ortiz-Lazareno PC. Daneri-Navarro, A. Low NKp30, NKp46 and NKG2D expression and reduced cytotoxic activity on NK cells in cervical cancer and precursor lesions. BMC Cancer. 2009;9:1–8.
38. Han B, Mao F-y, Zhao Y-l, Lv Y-p, Teng Y-s, Duan M, Chen W, Cheng P, Wang T-t, Liang Z-. y. Altered NKp30, NKp46, NKG2D, and DNAM-1 expression on circulating NK cells is associated with tumor progression in human gastric cancer. *Journal of immunology research* 2018, *2018*.
39. Busse D, de la Rosa M, Hobiger K, Thurley K, Flossdorf M, Scheffold A, Höfer T. Competing feedback loops shape IL-2 signaling between helper and regulatory T lymphocytes in cellular microenvironments. Proc Natl Acad Sci. 2010;107:3058–63.
40. Thibaut R, Bost P, Milo I, Cazaux M, Lemaître F, Garcia Z, Amit I, Breart B, Cornuot C, Schwikowski B. Bystander IFN-γ activity promotes widespread and sustained cytokine signaling altering the tumor microenvironment. Nat cancer. 2020;1:302–14.
41. Coppola L, Smaldone G, D'aiuto M, D'aiuto G, Mossetti G, Rinaldo M, Verticilo S, Nicolai E, Salvatore M, Mirabelli P. Identification of immune cell components in breast tissues by a multiparametric flow cytometry approach. Cancers (Basel). 2022;14:3869.
42. Park YH, Lal S, Lee JE, Choi Y-L, Wen J, Ram S, Ding Y, Lee S-H, Powell E, Lee SK. Chemotherapy induces dynamic immune responses in breast cancers that impact treatment outcome. Nat Commun. 2020;11:6175.
43. Kim R, Kawai A, Wakisaka M, Sawada S, Shimoyama M, Yasuda N, Hidaka M, Morita Y, Ohtani S, Arihiro K. Immune correlates of the differing pathological and therapeutic effects of neoadjuvant chemotherapy in breast cancer. Eur J Surg Oncol. 2020;46:77–84.
44. Harris MA, Savas P, Virassamy B, O'Malley MM, Kay J, Mueller SN, Mackay LK, Salgado R, Loi S. Towards targeting the breast cancer immune microenvironment. Nat Rev Cancer. 2024;24:554–77.
45. Rezaeifard S, Talei A, Shariat M, Erfani N. Tumor infiltrating NK cell (TINK) subsets and functional molecules in patients with breast cancer. Mol Immunol. 2021;136:161–7.
46. Bouzidi L, Triki H, Charfi S, Kridis WB, Derbel M, Ayadi L, Sellami-Boudawara T, Cherif B. Prognostic value of natural killer cells besides tumor-infiltrating lymphocytes in breast cancer tissues. Clin Breast Cancer. 2021;21:e738–47.
47. Gauthier L, Morel A, Anceriz N, Rossi B, Blanchard-Alvarez A, Grondin G, Trichard S, Cesari C, Sapet M, Bosco F. Multifunctional natural killer cell engagers targeting NKp46 trigger protective tumor immunity. Cell. 2019;177:1701–13. e1716.
48. Stankovic B, Bjørhovde HAK, Skarshaug R, Aamodt H, Frafjord A, Müller E, Hammarström C, Beraki K, Bækkevold ES, Woldbæk PR. Immune cell composition in human non-small cell lung cancer. Front Immunol. 2019;9:3101.
49. Wu J, Mishra HK, Walcheck B. Role of ADAM17 as a regulatory checkpoint of CD16A in NK cells and as a potential target for cancer immunotherapy. J Leukoc Biol. 2019;105:1297–303.
50. Hatjiharissi E, Xu L, Santos DD, Hunter ZR, Ciccarelli BT, Verselis S, Modica M, Cao Y, Manning RJ, Leleu X. Increased natural killer cell expression of CD16, augmented binding and ADCC activity to rituximab among individuals expressing the FcγRIIIa-158 V/V and V/F polymorphism. Blood J Am Soc Hematol. 2007;110:2561–4.
51. Muntasell A, Servitja S, Cabo M, Bermejo B, Pérez-Buira S, Rojo F, Costa-García M, Arpí O, Moraru M, Serrano L. High numbers of circulating CD57 + NK cells associate with resistance to HER2-specific therapeutic antibodies in HER2 + primary breast cancer. Cancer Immunol Res 2019.
52. Tang F, Li J, Qi L, Liu D, Bo Y, Qin S, Miao Y, Yu K, Hou W, Li J. A pan-cancer single-cell panorama of human natural killer cells. Cell. 2023;186(4235–4251):e4220.
53. Netskar H, Pfefferle A, Goodridge JP, Sohlberg E, Dufva O, Teichmann SA, Brownlie D, Michaëlsson J, Marquardt N, Clancy T. Pan-cancer profiling of tumor-infiltrating natural killer cells through transcriptional reference mapping. Nat Immunol. 2024;25:1445–59.
54. Chiossone L, Dumas P-Y, Vienne M, Vivier E. Natural killer cells and other innate lymphoid cells in cancer. Nat Rev Immunol. 2018;18:671–88.
55. Gao Y, Souza-Fonseca-Guimaraes F, Bald T, Ng SS, Young A, Ngiow SF, Rautela J, Straube J, Waddell N, Blake SJ. Tumor immunoevasion by the conversion of effector NK cells into type 1 innate lymphoid cells. Nat Immunol. 2017;18:1004–15.
56. Carrega P, Morandi B, Costa R, Frumento G, Forte G, Altavilla G, Ratto GB, Mingari MC, Moretta L, Ferlazzo G. Natural killer cells infiltrating human nonsmall-cell lung cancer are enriched in CD56brightCD16 – cells and display an impaired capability to kill tumor cells. Cancer. 2008;112:863–75.
57. Schmidt L, Eskiocak B, Kohn R, Dang C, Joshi NS, DuPage M, Lee D-Y, Jacks T. Enhanced adaptive immune responses in lung adenocarcinoma through natural killer cell stimulation. Proc Natl Acad Sci. 2019;116:17460–9.
58. Garrido MA, Rodriguez T, Zinchenko S, Maleno I, Ruiz-Cabello F, Concha Á, Olea N, Garrido F, Aptsiauri N. HLA class I alterations in breast carcinoma are

associated with a high frequency of the loss of heterozygosity at chromosomes 6 and 15. Immunogenetics. 2018;70:647–59.
59. Silva GBRFd, Silva TGA, Duarte RA, Neto NL, Carrara HHA, Donadi EA, Gonçalves MAG, Soares EG, Soares CP. Expression of the classical and nonclassical HLA molecules in breast cancer. *Int. J. Breast Cancer* 2013, *2013*.
60. Pinto S, Pahl J, Schottelius A, Carter PJ, Koch J. Reimagining antibody-dependent cellular cytotoxicity in cancer: the potential of natural killer cell engagers. Trends Immunol. 2022;43:932–46.
61. Sarkar S, Germeraad WT, Rouschop KM, Steeghs EM, van Gelder M, Bos GM, Wieten L. Hypoxia induced impairment of NK cell cytotoxicity against multiple myeloma can be overcome by IL-2 activation of the NK cells. PLoS ONE. 2013;8:e64835. https://doi.org/10.1371/journal.pone.0064835.
62. Van Berckelaer C, Rypens C, Van Dam P, Pouillon L, Parizel M, Schats K, Kockx M, Tjalma W, Vermeulen P, Van Laere S. Infiltrating stromal immune cells in inflammatory breast cancer are associated with an improved outcome and increased PD-L1 expression. Breast Cancer Res. 2019;21:1–12.
63. Pelekanou V, Barlow WE, Nahleh ZA, Wasserman B, Lo Y-C, von Wahlde M-K, Hayes D, Hortobagyi GN, Gralow J, Tripathy D. Tumor-infiltrating lymphocytes and PD-L1 expression in pre-and posttreatment breast cancers in the SWOG S0800 phase II neoadjuvant chemotherapy trial. Mol Cancer Ther. 2018;17:1324–31.
64. McNamara KL, Caswell-Jin JL, Joshi R, Ma Z, Kotler E, Bean GR, Kriner M, Zhou Z, Hoang M, Beechem J. Spatial proteomic characterization of HER2-positive breast tumors through neoadjuvant therapy predicts response. Nat cancer. 2021;2:400–13.

Publisher's note